Detailed defect study in proton irradiated InP/Si solar cells

R. J. Walters[a)]
Naval Research Laboratory, Code 6615, 4555 Overlook Ave., S.W., Washington, DC 20375

M. J. Romero, D. Araújo, and R. García
Departamento de Ciencia de los Materiales e I.M. y Q.I., Facultad de Ciencias, Universidad de Cádiz, Apdo. 40, E-11510, Puerto Real (Cádiz), Spain

S. R. Messenger
SFA, Inc, Largo, Maryland 20774

G. P. Summers
Naval Research Laboratory, Code 6615, 4555 Overlook Ave., S.W., Washington, DC 20375
and Department of Physics, University of Maryland Baltimore County, Baltimore, Maryland 22125

(Received 22 February 1999; accepted for publication 25 June 1999)

A detailed study of the effects of proton irradiation-induced defects in heteroepitaxially grown InP/Si solar cells has been made through a combination of cathodoluminescence (CL), electron beam induced current (EBIC), and electrochemical capacitance versus voltage (ECV) carrier profiling measurements. The CL data indicate the distribution of nonradiative recombination centers both before and after proton irradiation, and temperature dependent and spectroscopic analysis of the CL signal give an estimate of the energies of the dominant defect levels. The EBIC data yield an estimate of the magnitude and spatial variation of the minority carrier diffusion length (L) in the base region. Values of L determined from EBIC measurements made on solar cells irradiated by protons ranging in energy from 0.1 up to 4.5 MeV follow a single curve when plotted versus displacement dose, D_d, allowing a single proton damage coefficient to be determined. The ECV measurements show the evolution of the carrier concentration profile in the cell under irradiation, as carrier removal first depletes and eventually type converts the base region. From an in-depth analysis of the combined data, the physical defects that give rise the radiation-induced energy levels are suggested, and a detailed understanding of the physical mechanisms causing the radiation response of InP/Si solar cells is developed.
[S0021-8979(99)05019-7]

I. INTRODUCTION

From cost and operational viewpoints, it appears advantageous to locate global coverage satellite communication systems in orbits near or in the proton radiation belts, which extend from approximately 2000 to 10 000 km above the earth's surface. However, radiation effects are very severe in these orbits, and currently, InP solar cells offer one of the few possible options for the power system of such satellites. InP solar cells grown on Si substrates (InP/Si) combine the superior radiation resistance of InP with the strength and cost effectiveness of Si. These cells show essentially no degradation even after proton and electron irradiation up to fluences equivalent to more than 1×10^{16}, 1 MeV electrons cm^{-2}. The challenge facing InP/Si cell technology, however, is the growth of high beginning-of-life cells. Although InP cells grown on InP substrates can achieve efficiencies $>19\%$ (AM0), the lattice mismatch between InP and Si leads to the formation of threading dislocations that propagate into the active regions of InP/Si cells (Fig. 1). Currently, InP/Si cells can be grown with efficiencies around $\sim13\%$.[1]

In an effort to understand the detailed physical mechanisms responsible for the radiation response of InP/Si and other advanced space solar cells, a collaborative research program has been established between the U.S. Naval Research Laboratory (NRL) and the University of Cadiz, Cadiz, Spain. In this program, electron beam induced current (EBIC) and cathodoluminescence (CL) measurements are combined with spectral response and electrochemical, capacitance versus voltage (ECV) studies to measure radiation-induced changes in carrier concentration, diffusion length and defect distributions in solar cells. These results can then be compared to photovoltaic measurements made on the same cells. This article reports initial results from this research.

II. EXPERIMENTAL DETAILS

Spire Corporation grew the InP/Si solar cells studied here under contract to the NRL (Fig. 2). These are n^+p shallow homojunctions grown epitaxially by metalorganic chemical vapor deposition (MOCVD) on 12-mil-thick, n-type Si wafers. The cells have very thin emitters (~250 Å thick) of heavily Si doped n-type InP. The p-type base region is ~1.5-μm-thick and doped to $\sim5\times10^{16}\,cm^{-3}$ with Zn with a ~1.5-μm-thick back surface field (BSF) region. The InP thermal buffer layer is grown to reduce the dislocation density. The InGaAs tunnel junction is required because of

a)Electronic mail: rwalters@ccf.nrl.navy.mil

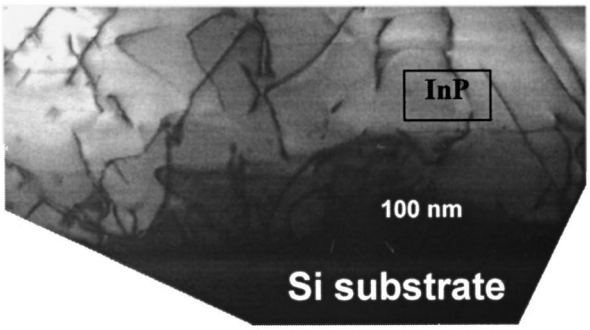

FIG. 1. Transmission electron microscopy micrograph of an InP/Si solar cell. This image shows the threading dislocations that propagate into the cell active layers from the interface due to the ~8% lattice mismatch between InP and Si.

the formation of an opposing diode at the back of the cell by the out-diffusion of Si from the substrate during growth. The cell area was 1×1 cm^2.

The solar cells were exposed to monoenergetic, normal incidence proton irradiation through the front surface using the Peletron Accelerator facility at the Naval Surface Warfare Center at White Oak, Maryland. The proton energy ranged from 0.1 to 4.5 MeV. The fluence was determined from the total charge striking the target plane using a current integrator. The accuracy of the dosimetry in all cases was about 10%. For analysis, the fluence was converted to displacement damage dose,[2] D_d, by multiplying by the appropriate nonionizing energy loss for protons in InP.

For the CL and EBIC measurements, the cells were mounted in a JEOL–JSM820 scanning electron microscope (SEM). CL measurements were made between 60 and 300 K on freshly cleaved {110} faces perpendicular to the epilayers of a cell (Fig. 3). To monitor the luminescence, micrographs and spectra were recorded from different locations within the InP buffer and base regions of the cell (Figs. 1 and 2). A semi-parabolic mirror attached to an optical guide yielded highly efficient collection of the luminescence. A cryogenic change coupled device array (Photometrics SDS9000) was attached to an Oriel 77400 spectrograph/monochromator for spectroscopic analysis of the CL. A CTI-Cryogenics 22C/350C closed-cycle, liquid He cryostat attached to an antivibration system was used in making low temperature CL measurements.

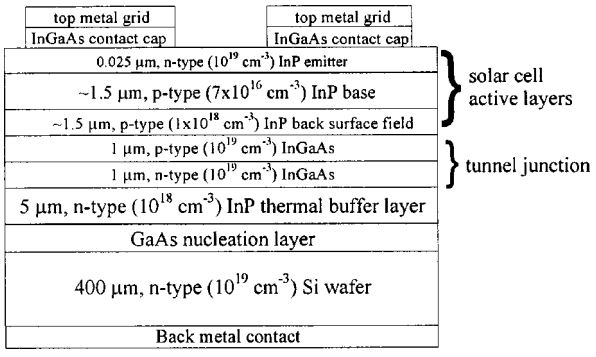

FIG. 2. Schematic cross-section diagram of an InP/Si solar cell.

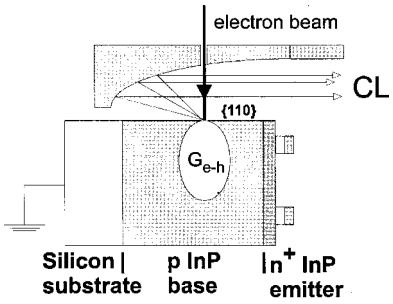

FIG. 3. Configuration of the CL measurements made within a JEOL–JSM820 SEM. The electron beam was incident on a freshly cleaved {110} face, oriented perpendicular to the cell epilayers.

The experimental arrangement for making EBIC measurements is shown schematically in Fig. 4. Prior to loading a cell into the SEM, the cell was mounted on a holder that had been modified so pressure could be applied to the front and rear contacts. The electron beam induced current (I_{cc}) was detected using a head amplifier and a low input-impedance MATELECT ISM-5A amplifier and MATELECT IU-1 computer interface. Use of the MATELECT ISM-5A to detect photogenerated current assisted in ensuring a good contact to the cell. The incident electron beam current (I_b) was measured by a Faraday cup. The EBIC gain is defined as (I_{cc}/I_b). The electron beam energy (E_b) was varied from 1 to 30 keV. Analysis of the EBIC data is discussed in the Appendix.

The ECV profiles were measured using Polaron Profiler.

III. EXPERIMENTAL RESULTS

A. CL

Figure 5(a) shows a CL micrograph measured on an unirradiated InP/Si cell with the electron beam located over the InP buffer layer at the rear of the cell (Figs. 1 and 2). The signal is seen to be highly nonuniform, indicating the presence of a spatially varying distribution of nonradiative recombination centers. At 60 K the CL emission from the cell was spectroscopicly resolved into two peaks at 1.38 and 1.414 eV (Fig. 6). The emission peak at 1.414 eV was observed in all the cells both before and after irradiation and can be attributed to the free-to-bound recombination (h,D^0) related to the Si donor, with an impurity energy level of 6–7 MeV, obtained from the Eagles distribution.[3] The depen-

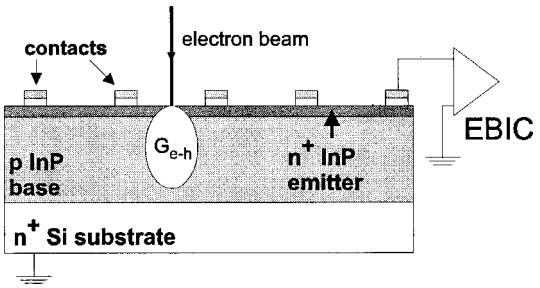

FIG. 4. Sample mounting configuration for EBIC measurements. As for the CL measurements, these measurements were made within a JEOL–JSM820 SEM.

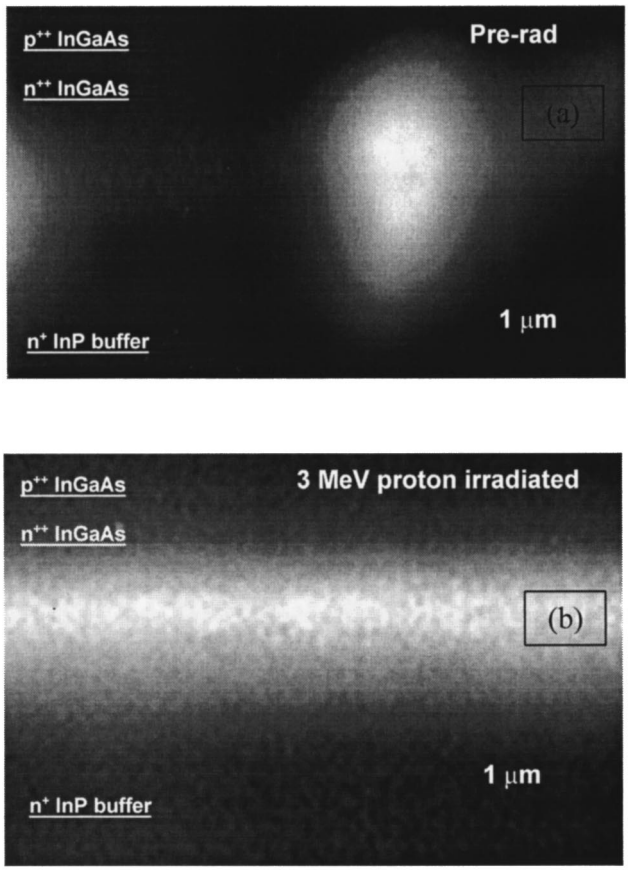

FIG. 5. CL micrographs taken of InP/Si solar cells at 300 K before (a) and after (b) 3 MeV proton irradiation up to $D_d = 2.6 \times 10^{12}$ MeV/g. The electron beam was incident on the InP buffer region (see Figs. 1 and 2). Prior to irradiation, the variation in luminescence intensity across the sample is a result of the nonuniform distribution of nonradiative defects associated with threading dislocations. Following proton irradiation, the CL is uniform, indicating a uniform distribution of radiation-induced, nonradiative defects.

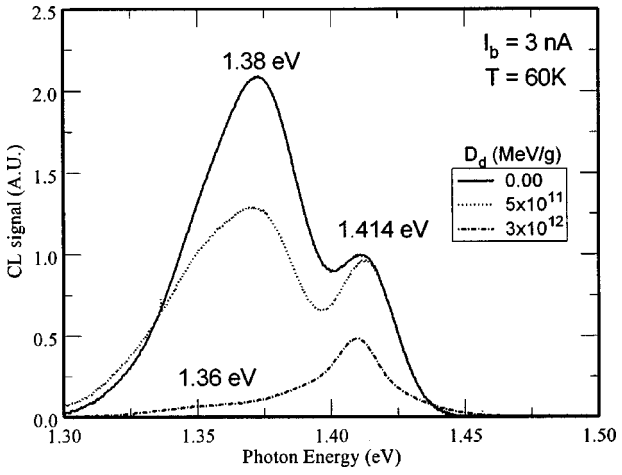

FIG. 6. Spectroscopic analysis of the CL data measured at 60 K in InP/Si cells both before and after proton irradiation. Prior to irradiation, two main peaks are observed at 1.414 and 1.38 eV, respectively. The irradiation causes the intensity of the 1.38 eV peak to be significantly reduced. As the 1.38 eV signal decreases, a broad peak near 1.36 eV emerges. The CL intensity for each spectrum is arbitrary and has been normalized to the height of the 1.414 eV peak measured before irradiation.

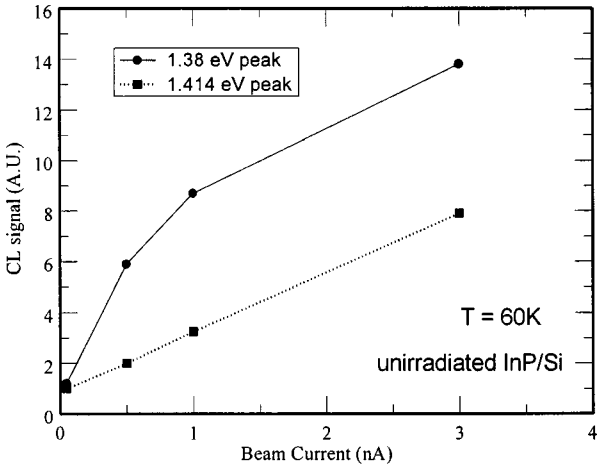

FIG. 7. Dependence of the CL peak intensity cell on the electron beam current (I_b) measured in an unirradiated InP/Si solar cell. The increase in the 1.38 eV signal is nonlinear, suggesting either a change in slope or saturation of the emission.

dence of the CL intensity on I_b is shown in Fig. 7. The intensity of the 1.414 eV peak appears to increase linearly with I_b as expected. The 1.38 eV peak intensity, however, does not. These data suggest either a change in slope at higher injection levels or saturation of the emission at the beam incidence point.

Proton irradiation was observed to cause an overall reduction in CL intensity due to the introduction of nonradiative recombination centers. Also, the irradiations caused the CL signal to become more spatially uniform [Fig. 5(b)]. Spectroscopic resolution of the CL measurements made at 60 K on irradiated cells showed a reduction in, and essentially the removal of, the 1.38 eV peak (Fig. 6) with increasing D_d levels. In addition, a broad peak, centered at 1.36 eV emerged as a shoulder to the 1.38 eV peak. An increase in I_b caused a shift in the energy of this peak of about $+6$ MeV/nA.

The total integrated CL intensity measured in a 3 MeV proton irradiated cell is plotted as a function of inverse temperature, i.e., an Arrhenius plot, in Fig. 8. The data seem to exhibit three different exponential regions, indicating three different thermally activated, nonradiative recombination levels. However, there was a large scatter in the data for temperatures below ~120 K; so the shallowest defect level was ignored, and the data were analyzed in terms of two thermally activated processes, α and β, respectively. The emission efficiency, η, was approximated by the equation:[4]

$$\eta = \left[1 + \kappa^{\alpha} \exp\left(-\frac{E^{\alpha}}{k_B T} \right) + \kappa^{\beta} \exp\left(-\frac{E^{\beta}}{k_B T} \right) \right]^{-1}, \qquad (1)$$

where κ is the ratio of the radiative to the nonradiative recombination lifetimes at $T = 300$ K, and E is the thermal activation energy measured from the minority carrier band, i.e., the conduction band for the present p-type samples. The fit, shown as a solid line in Fig. 8, yielded $E^{\alpha} = 0.73$ eV, $E^{\beta} = 0.26$ eV, $\kappa^{\alpha} \sim 1 \times 10^{15}$, and $\kappa^{\beta} \sim 1 \times 10^{7}$.

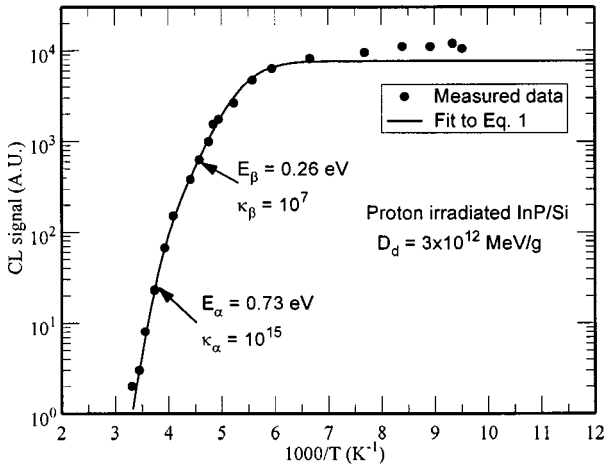

FIG. 8. Arrhenius plot of the CL intensity measured on a 3 MeV proton irradiated InP/Si solar cell. The solid line represents a fit of the data to Eq. (1) assuming two nonradiative recombination mechanisms.

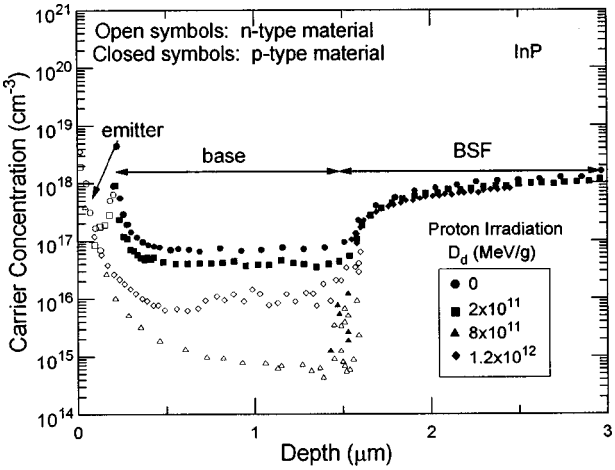

FIG. 10. Carrier concentration profiles measured by ECV on an InP/Si solar cell irradiated with 3 MeV protons. Carrier removal first causes the *p*-type base to become semi-insulating and then *n* type, so the cell structure evolves from n^+-p-p^+ to n^+-i-p^+ and finally to n^+-n-p^+. The junction is ultimately pushed back to the base/BSF interface.

B. EBIC

EBIC measurements were made on the proton irradiated cells. From these measurements, an estimate of L was determined for each of the cells. A plot of L vs D_d is shown as open squares in Fig. 9. Another estimate of L vs D_d was determined from spectral response (quantum efficiency) measurements made on a cell irradiated with incremental fluences of 3 MeV protons. In this case, L was determined from fits of the spectral response data to the equations of Hovel.[5] These results are plotted as closed squares in Fig. 9, where it can be seen that they agree very well with the EBIC measurements.

The data shown in Fig. 9 were fitted to the diffusion length degradation equation[6]

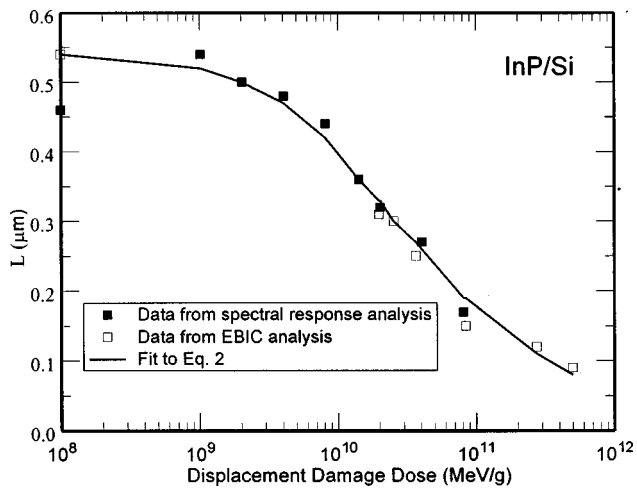

FIG. 9. A plot of the minority carrier diffusion length (L) in the base region of InP/Si cells vs displacement damage dose. Results determined from both EBIC and spectral response measurements are shown. The measurements were made on cells irradiated with monoenergetic protons ranging in energy from 0.1 up to 4.5 MeV. Displacement damage dose is the product of the proton fluence and the nonionizing energy loss (see Ref. 2). The continuous line is a fit of the data to Eq. (2).

$$\frac{1}{L^2(D_d)} = \frac{1}{L_0^2} + K_L D_d, \tag{2}$$

where L_0 is the pre-irradiation value of L, and K_L is the proton diffusion length damage coefficient. The fit gave a value for L_0 of $0.56 \pm 0.14\,\mu$m and for K_L of $2.93 \pm 0.55 \times 10^{-10}$ g/(cm^2 MeV).

C. ECV

Figure 10 shows the ECV profile measured on an InP/Si solar cell under proton irradiation. Figure 10 shows the polarity and carrier concentration measured from the front of the cell to a depth of 3 μm. The emitter region is so thin that it is not apparent in the figure. Prior to irradiation, the base region is p type with a carrier concentration of $\sim 8 \times 10^{16}$ cm^{-3}. Beyond the base is a heavily doped p-type BSF region (Fig. 2). Carrier removal in p-type InP is independent of the initial carrier concentration, so that proton irradiation causes effects that are apparent only in the relatively lightly doped base region.[7] It can be seen that proton irradiation caused the hole concentration in the p-type base region to decrease. At higher D_d levels, the base region is type converted so that the emitter effectively extended from the front of the cell to the BSF region. When D_d exceeded 8×10^{11} MeV/g, the base was driven even more n type so that the cell structure had evolved from n^+-p-p^+ to n^+-i-p^+ and eventually to n^+-n-p^+. At the final stage, the junction was formed between the n-type ''base'' and the heavily doped p-type BSF region.

IV. DISCUSSION

A. Solar cell radiation-induced degradation

One of the primary damage mechanisms in a solar cell due to particle irradiation is degradation of the minority carrier diffusion length, L.[6] Figure 9 shows that a single curve is produced when radiation-induced reductions in L, determined both from EBIC and spectral response measurements,

are plotted versus D_d for a range of incident proton energies. A single proton damage coefficient can therefore be determined, which is independent of proton energy. These results indicate that the degradation of L by proton irradiation at any energy, or even under irradiation by a known spectrum of protons as is often encountered in a space radiation environment, can be accurately predicted using this single damage coefficient. This result is consistent with the model of Summers, Burke, and Xapsos,[2] in which the response of a solar cell to irradiation by protons of various energies can be described by a single, characteristic curve in terms of D_d. These new results further indicate the usefulness of the displacement damage dose model.

The degradation of L in a solar cell is primarily caused by radiation-induced deep levels acting as trapping and recombination sites. The CL data analysis identified the dominant recombination center (i.e., the α center) to lie at 0.73 eV below the conduction band. This defect could be identified with the radiation-induced, minority carrier trap labeled EB (E_c-0.74 eV) that has been characterized by deep level transient spectroscopy (DLTS) studies of irradiated InP.[8] However, the EB DLTS peak is completely removed by thermal annealing at temperatures as low as 330 K[9] with essentially no recovery in solar cell performance. Also, one would not expect to detect the α center as a minority carrier trap by DLTS since it acts as a recombination center. Instead, the α center may more likely be identified with the DLTS peak labeled H5 ($E_v+0.54$ eV). Although H5 is detected as a majority carrier trap, it has also been shown to be an efficient recombination center,[10] so the α center could be the minority carrier trapping level corresponding to the H5 defect. This conclusion is consistent with the results of Refs. 1 and 11 where the H5 defect level was found to strongly control the radiation response and annealing properties of InP solar cells.

Carrier removal effects have also been shown to be important in the radiation response of the InP/Si solar cells, causing the ultimate collapse of the cell at high fluence levels.[12] Indeed, the ECV measurements presented here showed severe carrier removal that eventually type converted the cell base. The β center (Fig. 8) is expected to play a role in this behavior since, the location of its energy level ($E_c-0.26$ eV), suggests that it will act as a compensation center. This defect may possibly be identified with the radiation-induced DLTS peak labeled EA.[8] Such a conclusion is in agreement with the results of Ref. 11 where the lack of recovery of the carrier concentration in irradiated InP solar cells after thermal annealing was associated with the persistent presence of the EA peak along with the minority carrier traps labeled EC and ED.

B. Analysis of the CL spectral peaks

Even though the CL data were taken from the *n*-type InP buffer layer that was not intentionally doped with Zn, the 1.38 eV CL peak (Fig. 6) appears to be the conduction band-to-acceptor or shallow donor-to-acceptor transition (e/D–A) associated with Zn acceptors.[13,14] A significant concentration of Zn atoms is expected in the buffer layer due to MOCVD reactor memory effects and Zn diffusion along the threading dislocations.[14] Related to this is the observation that the spatial variation of the CL signal [Fig. 5(a)] is due primarily to the spatial variation of the 1.38 eV peak signal and could be related to the spatial distribution of the threading dislocations (Fig. 1). However, the 1.38 eV peak signal did not show the expected linear scaling with I_b,[14] suggesting, perhaps, a defect related transition. The photoluminescence experiments on heteroepitaxial InP reported by Olego *et al.*[15] indicate a defect-related luminescence peak in this energy range. If so, the defect could likely be a vacancy because a large number of vacancies are expected to exist in the highly mismatched InP on Si material and the dislocations will getter these vacancies.[16] Also, it is more likely that a P vacancy is involved rather than an In vacancy since the formation enthalpy of $V_{\mathrm{P}}(2.17\,\mathrm{eV})$ is significantly lower than that of $V_{\mathrm{In}}(3.04\,\mathrm{eV})$.[17,18] While the evidence at hand is not conclusive, it seems plausible that the 1.38 eV peak is produced by V_{P}–Zn acceptor complexes that form along the vacancy-decorated threading dislocations.

It should be noted that a contribution to the CL intensity from acceptor transitions related to the Si impurities is also possible. The InP buffer layer has a high Si concentration due to out diffusion from the wafer during cell growth. While Si typically replaces In to form a donor, clear evidence of amphoteric and acceptor behavior (impurity energy level of 37 MeV) of Si in InP has been reported,[19,20] so Si-acceptor related transitions are a distinct possibility.

Considering the 1.36 eV peak, Sieg, Chatterjee, and Ringel,[14] studying samples very similar to the present InP/Si solar cells, identified a similar peak as arising from an interstitial Zn donor to a substitutional Zn-acceptor (D–A) transition. The observed shift in the peak energy with an increase in I_b is a common signature of such a distant donor-to-acceptor pair transition,[21] but Sieg, Chatterjee, and Ringel[14] observed this peak in as-grown samples while the present data suggest that this peak may be introduced by the proton irradiation. Alternatively, ion implantation of InP has been observed to introduce a broad CL peak near 1.36 eV similar to that observed here[13,22–24] that has been identified as a defect induced donor level (~33 MeV)-Zn-acceptor transition. In this case, Si was found to not be directly involved with the emission centers and even suppressed them.[13] The identity of the defect is not known, but the fact that it was observed following Al, P, and Si irradiation, suggests a native defect or a related complex. Beryllium irradiation, however, does not induce this peak, which suggests a defect complex,[13,17] and since the peak is seen after irradiation by column III or V ions, it is probably not a simple vacancy. The dominant defect in *n*-type InP, other than a simple vacancy, is the In antisite defect ($\mathrm{In_P^{2-}}$).[25] This is supported by the fact that antisite defects are reported to be stable in III–V compounds.[26,27] This is further supported by the fact that B. Massarani and J. C. Bourgoin[28] have shown the H5 DLTS peak to be caused by displacements on the In sublattice, which correlates directly to the preceding analysis of the solar cell degradation. Therefore, the CL band at 1.36 eV is tentatively assigned to a radiation-induced D–A transition produced by an $\mathrm{In_P^{2-}}$–Zn defect complex.

V. SUMMARY

A detailed analysis of the defect levels in InP/Si solar cells both before and after proton irradiation has been presented. The primary radiation-induced solar cell degradation mechanisms are a decrease in the minority carrier diffusion length, L, and carrier removal in the p-type cell base. Diffusion length degradation data measured following irradiation by protons of different energies were found to correlate directly in terms of displacement damage dose, D_d, so that a single damage coefficient could be determined to describe the cell response to any proton radiation environment. The data suggest the degradation of L to be primarily due to a radiation-induced recombination level found at E_c-0.73 eV that has been tentatively identified with the H5 DLTS peak. The data suggest that the carrier removal is caused primarily by a radiation-induced compensation center found at E_c-0.26 eV that has been tentatively identified with the EA DLTS peak. Spectral analysis of the CL data suggested that the primary radiation-induced defect may be an In antisite ($\mathrm{In_P^{2-}}$)–Zn defect complex which gives rise to these two energy levels and thus controls the solar cell radiation response.

ACKNOWLEDGMENTS

This work was supported in Spain by the CICYT (Comisión Interministerial de Ciencia y Tecnología) under MAT94-0823-CO3-02 and by the Junta de Andalucáia through group TEP-0120. The U.S. Office of Naval Research provided partial support of the work at the NRL.

APPENDIX

The operation of a semiconductor device is described by a set of three coupled partial differential equations. These equations are the Poisson equation for the electrostatic potential,

$$\nabla^2\phi = -\frac{e}{\epsilon_s}(p - n + N_d^+ - N_a^-) \tag{A1}$$

and the electron and hole current continuity equations (drift-diffusion model)

$$\nabla \mathbf{J}_n = e(R-G), \mathbf{J}_n = e(-\mu_n n \nabla\phi + D_n \nabla n), \tag{A2}$$

$$\nabla \mathbf{J}_p = -e(R-G), \mathbf{J}_p = e(-\mu_p p \nabla\phi - D_p \nabla p). \tag{A3}$$

In the EBIC and CL experiments, the local carrier excitation of the e beam is inserted in the electron-hole continuity equations as a carrier generation term G (estimated from a Monte Carlo procedure) and then the set of equations is solved. Therefore, the EBIC and CL signals of the semiconductor device is simulated and, by comparison with the experimental data, transport parameters (as the minority carrier diffusion length) can be fitted with the high spatial (submicron) resolution of these techniques. To resolve the steady-state semiconductor device Eqs. (A1)–(A3), we make use of the discretisation scheme from C. E. Korman and I. D. Mayergoyz,[29] partially modified by W. W. Keller[30] applied on the G. J. L Ouwerling[31] mesh design from the successive over relaxation method, to increase the convergence rate.

[1] R. J. Walters, S. R. Messenger, H. L. Cotal, M. A. Xapsos, S. J. Wojtczuk, H. B. Serreze, and G. P. Summers, J. Appl. Phys. **82**, 2164 (1997).
[2] G. P. Summers, E. A. Burke, and M. A. Xapsos, Radiat. Meas. **24**, 1 (1995).
[3] D. M. Eagles, J. Phys. Chem. Solids **16**, 76 (1960).
[4] J. D. Lambkin, L. Considine, S. Walsh, G. M. O'Connor, C. J. McDonagh, and T. J. Glynn, Appl. Phys. Lett. **65**, 73 (1994).
[5] H. J. Hovel, in *Semiconductors and Semimetals*, edited by R. K. Willardson and A. C. Beer (Academic, New York, 1975), Vol. 11, pp. 17–20.
[6] H. Y. Tada, J. R. Carter, B. E. Anspaugh, and R. G. Downing, *The Solar Radiation Handbook* (NASA JPL Publication 82–69, 1982).
[7] S. R. Messenger, R. J. Walters, M. A. Xapsos, G. P. Summers, and E. A. Burke, IEEE Trans. Nucl. Sci. **45**, 2857 (1998).
[8] R. J. Walters and G. P. Summers, J. Appl. Phys. **69**, 6488 (1991).
[9] M. J. Panunto, Doctoral Dissertation, University of Maryland, Baltimore County, 1996.
[10] S. W. S. McKeever, R. J. Walters, S. R. Messenger, and G. P. Summers, J. Appl. Phys. **69**, 1435 (1991).
[11] R. J. Walters, S. R. Messenger, H. L. Cotal, and G. P. Summers, J. Appl. Phys. **80**, 4315 (1996).
[12] S. R. Messenger, M. A. Xapsos, R. J. Walters, H. L. Cotal, S. J. Wojtczuk, H. B. Serreze, and G. P. Summers, Proceedings of the 26th IEEE Photovoltaic Specialists Conference, Anaheim, CA (1997), p. 995.
[13] T. S. Kim, S. D. Lester, and B. G. Streetman, J. Appl. Phys. **62**, 1363 (1987).
[14] R. M. Sieg, B. Chatterjee, and S. A. Ringel, Appl. Phys. Lett. **66**, 3108 (1995).
[15] D. J. Olego, Y. Okuno, T. Kawano, and M. Tamura, J. Appl. Phys. **71**, 4492 (1992).
[16] J. P. Hirth and J. Lothe, *Theory of Dislocations* (McGraw-Hill, New York, 1968), Chap. 18.
[17] M. V. Rao, J. Appl. Phys. **61**, 337 (1987).
[18] J. A. Van Vechten, J. Electrochem. Soc. **122**, 419 (1975).
[19] G. S. Pomrenke, J. Cryst. Growth **64**, 158 (1983).
[20] O. Ka, A. Yamada, H. Yoshinaga, and Y. Makita, J. Appl. Phys. **78**, 5171 (1995).
[21] R. Dingle, Phys. Rev. **184**, 788 (1969).
[22] P. K. Bhattacharya, W. H. Goodman, and M. V. Rao, J. Appl. Phys. **55**, 509 (1984).
[23] M. V. Rao, Appl. Phys. Lett. **48**, 1522 (1986).
[24] M. V. Rao, O. A. Aina, A. Fathimulla, and P. E. Thompson, J. Appl. Phys. **64**, 2426 (1988).
[25] R. W. Jansen, Phys. Rev. B **41**, 7666 (1990).
[26] J. Schneider, in *Semi-insulating III-V Materials*, edited by S. Makram Ebeid and B. Tuch (Shiva, London, 1982), p. 144.
[27] T. A. Kennedy and N. D. Wilsey, Appl. Phys. Lett. **44**, 1089 (1984).
[28] B. Massarani and J. C. Bourgoin, Phys. Rev. B **34**, 2470 (1986).
[29] C. E. Korman and I. D. Mayergoyz, J. Appl. Phys. **68**, 1324 (1990).
[30] W. W. Keller, J. Appl. Phys. **61**, 5189 (1987).
[31] G. J. L. Ouwerling, J. Appl. Phys. **66**, 6144 (1989).